

# A 300-kHz 6.6-kW SiC Bidirectional LLC On-board Charger

Haoran Li, *Student Member, IEEE*, Zhiliang Zhang, *Senior Member, IEEE*, Shengdong Wang, Jiacheng Tang, Xiaoyong Ren, *Member, IEEE*, and Qianhong Chen, *Member, IEEE*

**Abstract**—The reverse LLC voltage gain is lower than unity. The DC-link voltage is then lower than the peak grid voltage so that the buck type DC-AC converters cannot be grid-tied directly, which causes the LLC reverse operation difficult in bidirectional application. This paper proposes a SiC bidirectional LLC charger architecture to achieve high efficiency and high power density. The first stage is an interleaved bridgeless totem pole PFC to achieve unity power factor. The second stage is a 300-kHz LLC taking advantage of wide ZVS range and magnetic integration. Thanks to extra control freedom of high DC-link voltage, the DC-DC voltage gain regulation is shared by the DC/AC stage taking advantage of high voltage SiC MOSFETs. A reverse LLC voltage gain compensation control by regulating DC-link voltage is proposed to enable the LLC bidirectional operation. A digital adaptive synchronous rectification driving scheme is proposed based on the LLC primary driver signals, which immunes to the circuit oscillation caused by high  $dv/dt$  and parasitic elements. A 6.6 kW SiC bidirectional LLC charger was built. The power density is 3.42 kW/L with 3 kW/kg and increases 55.6% over the reference design. The charging efficiency is above 96% through the battery voltage from 240 V to 420 V, and 2% higher than the state-of-the-art products. The peak discharging efficiency under 6.6 kW is 96%, and 1% higher than the state-of-the-art efficiency.

**Index Terms:** Charger, Electric vehicle/ Hybrid electric vehicle, LLC converter; SiC, Bidirectional, on-board charger, high frequency

## I. INTRODUCTION

As the Plug-in Hybrid Electric Vehicles (PHEVs) and Electric Vehicles (EVs) are friendly to the environment, they have gained high popularity [1]-[2]. Their batteries can be charged directly from the wall socket through an on-board or off-board charger, as shown in Fig. 1 [3]. In recent years, the portable off-board single-phase chargers have been attractive. They are featuring much lower product cost since they only need to meet the industrial standard instead of the automobile standard. Therefore, it is extremely important to

Manuscript received Oct. 30, 2018; revised Jan 4, 2019 and Mar. 12, 2019; accepted Mar. 25, 2019. This work was supported by the National Key Research and Development Program of China (2018YFB0904101), and Science and Technology Project of State Grid (SG SGHB0000KXJS1800685).

The authors are with the Aero-Power Sci-Tech Center, Nanjing University of Aeronautics and Astronautics, Nanjing 210016, Jiangsu, China (e-mail: Haorani1991@nuaa.edu.cn; zlzheng@nuaa.edu.cn; wangs@nuaa.edu.cn; tjc325@nuaa.edu.cn, renxy@nuaa.edu.cn; chenq@nuaa.edu.cn).

achieve high efficiency and compact size to obtain the portable characteristic.

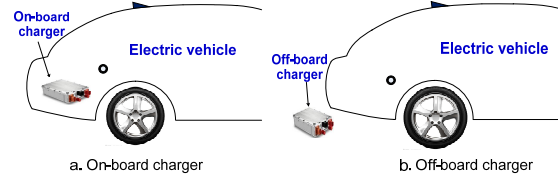


Fig. 1. Two charging methods for electric vehicles

Moreover, vehicle-to-grid (V2G) has drawn significant attention due to the increasing numbers of PHEVs and EVs, which can serve as moving storage units [4]. The discharging performance increases the flexibility for feeding the battery energy back to the grid, as well as supports the standalone loads such as the urgent rescue or outdoor lighting. It is a growing demand to take advantage of the charger to utilize the EVs battery energy supporting the standalone loads or the power grid [5]. Therefore, bidirectional operation, high power density and high efficiency are extremely important for the portable off-board charger.

The LLC converters are well-known for high efficiency, compact size and wide range of ZVS and ZCS [6][7]. In [8], the LLC converters are investigated in the battery charging applications to achieve high efficiency. However, the maximum voltage gain of reverse LLC is unity. When the battery voltage is low, the DC-link voltage is low accordingly. As the DC-AC converter is a buck type converter, the DC-link voltage has to be higher than the peak grid voltage so that the DC-AC converter can be grid-tied [9]. This causes the conventional LLC converters are not suitable for reverse operation directly. In [10], the LLC operates as a DC-DC transformer and the output voltage is regulated by a bidirectional buck/boost converter. But the extra non-isolated converter increases the system cost, size and power loss. So additional methods are generally required to achieve bidirectional LLC operation.

On the other hand, in order to address the problem of LLC bidirectional operation, a CLLLC converter is derived by adding an LC pair on the secondary side of the LLC converter [11][12][13]. The CLLLC resonant topology is able to realize bidirectional operation of the on-board chargers around the resonant point to achieve high efficiency, however, it needs an extra LC resonant pair [14].

High power density is critical and essential for the chargers. The current products of chargers are mainly Si-based design and operate typically at less than 100 kHz switching frequency, which results in large profile of the passive components [15]. It is an effective solution to

achieve high power density by increasing the switching frequency to shrink the passive components size significantly. However, when increasing the switching frequency based on the Si design, the efficiency decreases dramatically since the switching loss, conduction loss (considering the positive junction temperature coefficient), the AC winding loss and core loss of the magnetic components increase seriously at the same time [16]. Fortunately, the wide-band-gap devices such as SiC and GaN have much better Figure of Merit (FOM). They are able to increase the efficiency and power density dramatically due to the faster switching transition time and higher switching frequency compared to the Si devices. Moreover, the SiC devices can operate at higher temperature, higher voltage/ current and exhibit lower specific resistivity [17]. Therefore, the SiC MOSFETs are promising for EV chargers that require extremely high efficiency and high density.

It is also a serious challenge to maintain high efficiency over the entire battery voltage range. In [18], a dual active bridge (DAB) converter is applied in the battery charger. The DAB converter is well-known for its bidirectional performance. However, the DAB turn-off current is always high that shows a low efficiency performance for the high turn-off loss. Besides, the Synchronous Rectifiers (SRs) are also very important for high efficiency. The current sensing based SR schemes are valid, but need additional current sensing components and induce large loss [19]. In [20], the SR driving scheme senses the SR MOSFET drain-source voltage and the externally adjustable minimum off-time helps to fight the ring induced by the PCB and other parasitic elements. However, the maximum measurable drain source voltage is limited to 200 V, which it cannot be used under high voltage. Hence, it is urgent to develop a SR scheme to increase the efficiency, which is also suitable for high voltage applications.

This paper proposes a SiC bidirectional LLC charger together with bidirectional operation, high power density and high efficiency by taking advantage of the SiC devices of high voltage/ frequency. A voltage gain compensation control is proposed to achieve bidirectional LLC. Moreover, a digital adaptive SR driving scheme based on the LLC primary driver signals is also presented to further improve the efficiency.

## II. PROPOSED BIDIRECTIONAL LLC CHARGER ARCHITECTURE

### A. Proposed Bidirectional LLC Charger

The proposed bidirectional charger is shown in Fig. 2. The first stage adopts an interleaved bridgeless totem pole PFC, which can handle high power and achieve high quality grid current. Q7 and Q8 in parallel with Q5 and Q6 are used to reduce the conduction loss and increase the charger efficiency. The LLC converter is used as the second stage taking advantage of its high efficiency and high power density.

It is noted that the forward LLC has buck/boost operation capability, but the maximum voltage gain of the reverse LLC is unity. Fortunately, owing to the extra control

freedom of DC-link voltage, a voltage gain compensation control is proposed. The reverse LLC voltage gain can be compensated by increasing the bus voltage, so the DC-AC inverter can be grid-tied. The compensation principle is shown in Fig. 3. It shifts the voltage regulation burden from the LLC to the PFC and achieves bidirectional function.

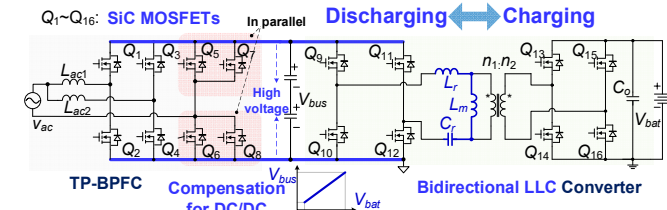


Fig. 2. Proposed bidirectional LLC charger architecture

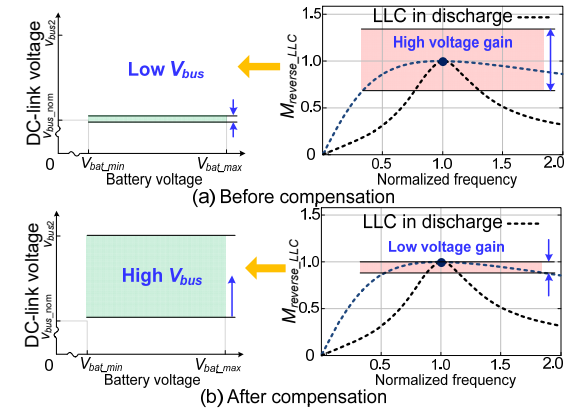


Fig. 3. Voltage gain compensation for reverse LLC in discharge

It should be noted that in the proposed control, the LLC switching frequency varies in a low range to eliminate the double-line frequency ripple, which is different from a DC transformer with a fixed switching frequency in [21]. Particularly, the proposed control regulates the DC-link voltage to track the full battery voltage range. But in [14], when the battery voltage is high, the DC-link voltage is regulated as a constant voltage. So the DC-DC stage still has to boost the output voltage by decreasing the switching frequency continuously. Therefore, the control process is absolutely different from this paper.

Furthermore, a digital adaptive SR driving scheme based on the primary driver signals is also proposed to improve the robust of SR driving signals. They are calculated directly in the DSP, which is different from the conventional SR scheme sensing the drain-source voltage or conduction current of power devices. So it immunes to the circuit oscillation caused by high  $dv/dt$  and the parasitic elements and is suitable for high voltage and high frequency applications.

In addition, an optimal LLC design is also presented to optimize the charger. The proposed design only considers the elimination of double-line frequency ripple and obtains the LLC magnetizing inductance as high as possible, which is different from the conventional LLC design.

### B. Charging and Discharging Mode

The proposed bidirectional LLC charger and the DC-DC equivalent circuits are shown in Fig. 4. In the charge as Fig. 4 (a), the LLC converter provides isolation and achieves wide range of ZVS and ZCS. Moreover, the magnetizing

inductance can be integrated in the transformer to obtain high power density.

In the discharge shown in Fig. 4 (b), the magnetizing inductance is in parallel with the battery voltage and not involved in the resonance. But the reactive current via the magnetizing inductance can help to achieve the ZVS and reduce the switching loss.

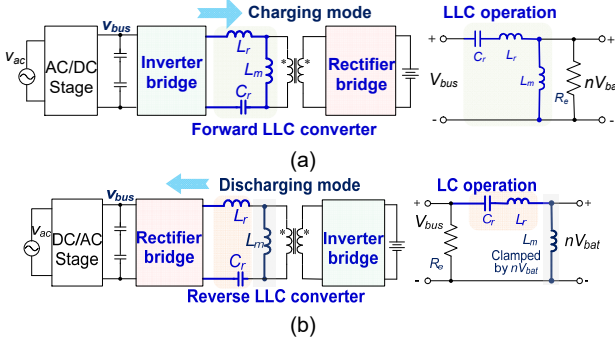


Fig. 4. Bidirectional charger and equivalent circuit (a) Charging mode (b) Discharging mode

### C. Advantages of Proposed Full SiC Charger

The proposed control regulates the DC-link voltage from 400 V to 700 V. Compared to the Si devices, the SiC devices can operate at higher voltage with lower resistivity and higher frequency.

TABLE I shows the power devices parameters of Si and SiC. The maximum DC-link voltage is 700 V, so that the withstand voltage is at least 900 V with nearly 30% margin. Compared with the Si MOSFETs, the SiC MOSFETs exhibit lower on-resistance with the same conduction current rating. So the SiC MOSFETs are more suitable for the proposed charger to obtain lower conduction loss and higher efficiency. The 1200 V SiC MOSFETs are also candidates for its lower on-resistance. As the battery voltage ranges from 240 V to 420 V, 650 V SiC MOSFET from ROHM is also a candidate that is suitable for the battery side.

TABLE I  
POWER DEVICES PARAMETERS OF SI AND SiC

MOSFET	Manufacturer	Part number	$V_{DSS}$	$I_D$	$R_{DS(on)}$ @75°C
Si	Infineon	IPW90R120C3	900 V	36 A	150 mΩ
	Wolfspeed	C3M0065090D	900 V	36 A	75 mΩ
SiC	Wolfspeed	C2M0040120D	1200 V	60 A	48 mΩ
	ROHM	SCT3022AL	650 V	93 A	25 mΩ

In order to achieve high power density, the LLC resonant frequency is designed as 300 kHz in the proposed charger to reduce the magnetic volume. The CoolMOS™ Si MOSFETs from Infineon can operate at 150 kHz.

Fortunately, the SiC devices can be used to push for high switching frequency. From Table I, 150-kHz Si MOSFETs and 300-kHz SiC MOSFETs are compared in the proposed charger topology and the chargers' efficiencies are evaluated in detail.

Fig. 5 demonstrates the power loss breakdown comparison between 900 V CoolMOS™ Si and 900 V SiC. In the high voltage application, the SiC charger has higher efficiency due to lower conduction loss and lower switching

loss. The charger efficiency comparison is given in Fig. 6 and the SiC charger efficiency is higher clearly.

Table II shows the magnetic cores selections in the two chargers. In the 300-kHz SiC charger, the transformer core volume is reduced by 36% and the resonant inductor core is reduced by 63% over 150-kHz Si charger. Consequently, the SiC devices make the proposed charger achieve higher efficiency and higher power density.

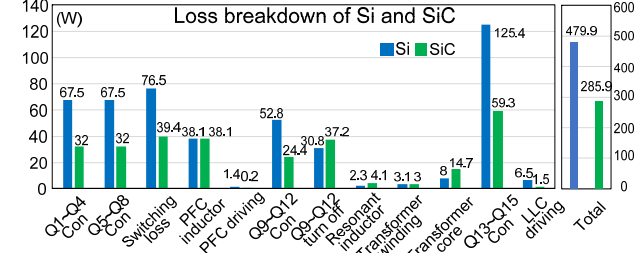


Fig. 5. Power loss comparison between Si and SiC of 900 V

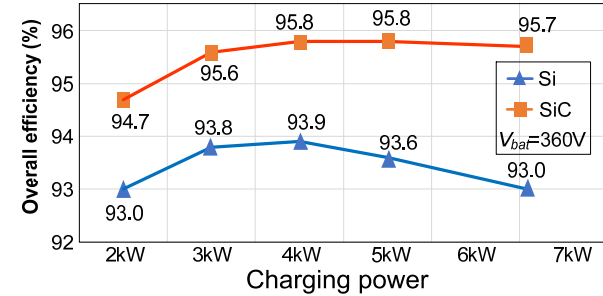


Fig. 6. Overall efficiencies comparison between Si and SiC of 900 V

TABLE II  
MAGNETIC CORES COMPARISONS OF SI AND SiC

	Si	SiC	Reduction
Switching frequency	150 kHz	300 kHz	-
Transformer core	ECW80	ECW64A	-
$L \times W \times H (\text{mm})$	77 × 68 × 31	64 × 50 × 33	36%
Resonant inductor core	EC55	EC45C	-
$L \times W \times H (\text{mm})$	55 × 26 × 55	44.9 × 32 × 20.2	63%
Material	DMR96	DMR96	-

### III. PROPOSED VOLTAGE GAIN COMPENSATION CONTROL

A voltage gain compensation control is presented to enable the LLC bidirectional function by increasing the DC-link voltage when the battery voltage increases. It is noted that the LLC is under Pulse Frequency Modulation (PFM) control and has to eliminate the double-line frequency ripple in a low switching frequency range instead of a DC transformer with a fixed switching frequency.

#### A. Proposed Control in Charging Mode

The voltage gain compensation control is shown in Fig. 8. The PFC stage adopts dual-loop control. The outer loop is the DC-link voltage control and the inner loop is the grid current control to achieve unity power factor and high quality grid current. The reference of the DC-link voltage is the product of the battery voltage and the transformer ratio. The reference of two inductor currents is from an identical signal that is the output of DC-link voltage control loop, so that two inductors current can be regulated identically to solve the current balancing problem.

In order to eliminate the double-line frequency ripple, the switching frequency is modulated in a low range that is less than 10% of the resonant frequency. Fig. 8 shows that when the battery voltage increases, the LLC loop gain almost has no changes due to the narrow switching frequency range, which simplifies the control design.

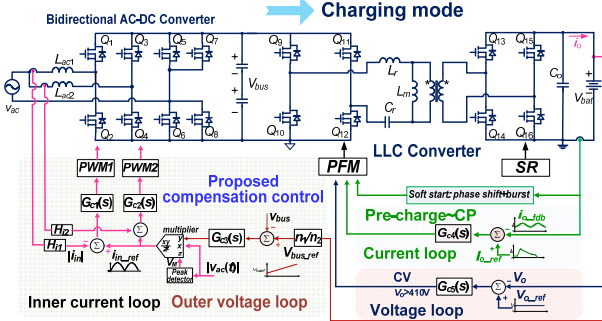


Fig. 7. Charging control diagram for proposed bidirectional charger

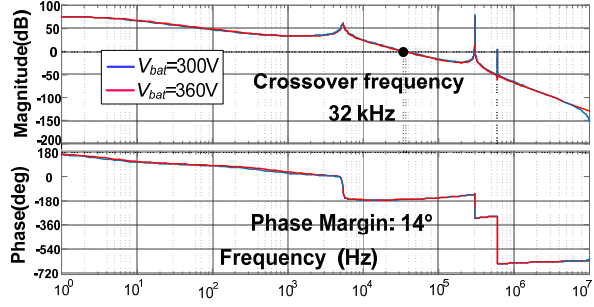


Fig. 8. LLC open loop bode diagram when battery voltages are 300 V and 360 V under 6.6 kW

### B. Proposed Control in Discharging Mode

The reverse LLC converter also adopts the voltage gain compensation control shown in Fig. 9. The switching frequency varies around the resonant frequency to obtain high efficiency. When the battery voltage is the minimum value of 240 V, the DC-link voltage is also 400 V so that the DC-AC inverter can be grid-tied in the entire battery voltage range. The DC-AC inverter adopts a grid-tied current loop to regulate the grid-tied power and achieve unity power factor. The grid-tied power is based on the battery output power.

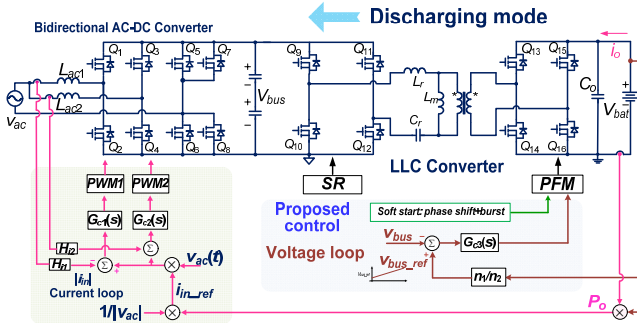


Fig. 9. Proposed discharging control diagram

## IV. PROPOSED ADAPTIVE DIGITAL SR DRIVING SCHEME

The proposed adaptive SR scheme is calculated based on the primary driving signals, which is directly from the Digital Signal Processor (DSP). It avoids the circuit

oscillations caused by high  $dv/dt$  and parasitic elements and is especially suitable for high voltage and high frequency application.

### A. Adaptive SR Driving Scheme

The proposed adaptive SR scheme is shown in Fig. 10. The SR algorithm is calculated based on the primary driving signals that are generated from the current loop or voltage loop. The turn-on delay time and turn-off time are initially calculated large enough, considering the worst condition including the non-linearities of the commutation, temperature variations and components tolerances. Therefore, there is enough safety margin of the dead time for the proposed SR driving scheme.

The LLC rectifier network is equivalent to a resistive load and the time delays do not affect the time domain model of the LLC converter. So the introduced time delays will not affect the closed control parameters design of the LLC.

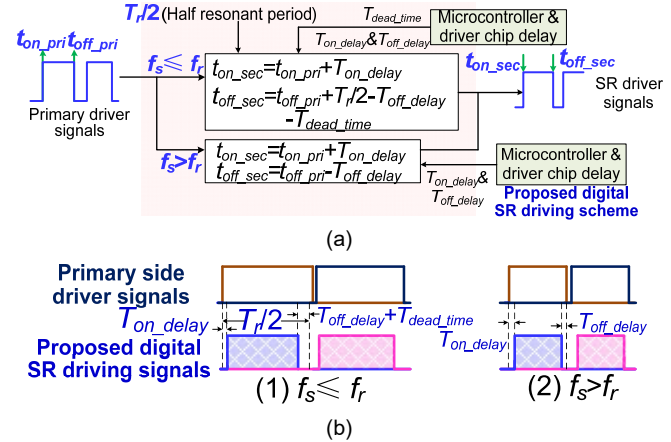


Fig. 10. Proposed digital SR driving scheme (a) SR algorithm flow (b) Driving signals waveforms

### B. SR Turn-on Time

The turn-on time of the secondary driving signals is identical to the primary driving signals. Considering the delays of microcontroller and driver chip, the turn-on time is derived as

$$t_{on\_sec} = t_{on\_pri} + T_{on\_delay} \quad (1)$$

where  $t_{on\_pri}$  and  $t_{on\_sec}$  denote the turn on time of the primary driving signals and secondary driving signals,  $T_{on\_delay}$  is the delay time.

### C. SR Turn-off Time

According to the resonant frequency  $f_r$  and the switching frequency  $f_s$ , the operation regions can be divided into three cases as  $f_s=f_r$ ,  $f_s < f_r$  and  $f_s > f_r$ . In the following sections,  $i_{Lm}$  denotes the magnetizing inductance current,  $i_{sec}$  is the secondary side current after rectification,  $i_{Lr}$  is the resonant current.

$$(1) f_s = f_r$$

At the resonant point, the secondary side current achieves critical ZCS. The conduction time of half wave is  $T_r/2$  ( $T_r$  denotes a resonant period). Considering the driver chip

delay  $T_{off\_delay}$  and the dead time  $T_{dead\_time}$ , the turn-off time at the resonant frequency is

$$\begin{aligned} t_{off\_sec} &= t_{off\_pri} - T_{off\_delay} \\ &= t_{on\_pri} + \frac{T_r}{2} - T_{dead\_time} - T_{off\_delay} \end{aligned} \quad (2)$$

(2)  $f_s < f_r$

As  $f_s$  is lower than  $f_r$ , there is a period of time that  $i_{Lr}$  circulates within the resonant tank without delivering power to the load. The secondary side MOSFETs turn off earlier than the primary side switches. So that the turn-off time is

$$t_{off\_sec} = t_{on\_pri} + \frac{T_r}{2} - T_{dead\_time} - T_{off\_delay} \quad (3)$$

According to (2) and (3), the two equations are identical. So when  $f_s \leq f_r$ , the SR turn-off time can be calculated using the same equation to simplify the control.

(3)  $f_s > f_r$

When the primary side MOSFETs turn off,  $i_{Lr}$  is unequal to  $i_{Lm}$  and still delivers power to the secondary side loads. When  $i_{Lm}$  is equal to  $i_{Lr}$ ,  $i_{sec}$  is zero. Then the turn-off time is

$$t_{off\_sec} = t_{off\_pri} - T_{off\_delay} \quad (4)$$

As a conclusion, the proposed digital SR driving scheme is shown in Fig. 10. Based on the primary driving signals, the SR driving signals can be determined by (1)~(4) which are calculated and accomplished in the DSP.

#### D. Considerations of Temperature Variations and Components Tolerances

The temperature variations or components tolerances mainly affect the resonance frequency drift. The resonance frequency is only used in the region when  $f_s \leq f_r$ .

A method to solve the problem is to increase the resonant frequency  $f_{r\_dsp}$  used in the DSP. The resonant period  $T_{r\_dsp}$  will decrease correspondingly shown in Fig. 11.  $f_{r\_dsp}$  is selected as the highest drifted resonance frequency. The method can not only achieve ZCS when the resonant tank parameters drift, but also guarantee light load ZCS since the actual SR conduction time under light load is lower than that under heavy load.

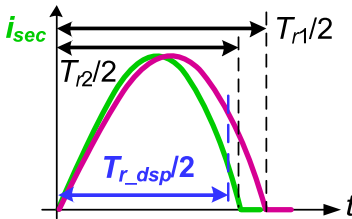


Fig. 11. Different resonant periods and DSP calculated period

#### V. OPTIMAL LLC DESIGN FOR PROPOSED BIDIRECTIONAL CHARGER

The point of the design is to obtain the LLC magnetizing inductance as high as possible and the LLC voltage gain should also be high enough to eliminate the double-line frequency ripple. Compared to the conventional LLC design,

the proposed design only needs to design a lower voltage gain in a lower switching frequency range.

#### A. Battery load Impact analysis

The battery load is simulated by the electronic load in this paper based on the charging profile shown in Fig. 12.

During  $T_1$ , the charging current is increased linearly from 16 A to 22 A. During  $T_2$ , when the battery voltage is 300 V, the charging current is 22 A. Then the battery is charged by the constant full power mode of 6.6 kW. During  $T_3$ , when the battery voltage approaches 420 V, the output voltage is regulated as the constant voltage mode of 420 V and the charging current is then limited.

The battery load is generally equivalent to a resistive load  $R_{eq}$  that varies in the charging process and the value is the battery voltage/ battery current. Firstly, the minimum  $R_{eq}$  ( $R_{eq\_min}$ ) corresponds to the point of the lowest battery voltage under full load, so that the double-line frequency ripple  $\Delta V_{dc}$  is maximum. Secondly,  $R_{eq\_min}$  also corresponds to the maximum quality factor  $Q_{max}$ , which results in the lowest LLC voltage gain. Therefore, the key is that the LLC voltage gain with  $Q_{max}$  and  $R_{eq\_min}$  should be high enough to eliminate the maximum  $\Delta V_{dc}$ .

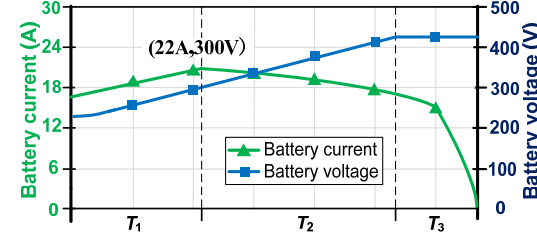


Fig. 12. Charging profile of proposed charger

#### B. LLC Optimal Design

From Fig. 12, the battery voltage ranges from 240 V~420 V. As the battery voltage is 300 V, the charging current is 22 A and the charging power is 6.6 kW, which corresponds to  $R_{eq\_min}$  equaling to 13.64 Ω. The LLC design is as follows.

1) The transformer turns ratio design. The turns ratio is determined by the minimum DC-link voltage (400 V is selected in this case) and the minimum battery voltage (it is 240 V in this case). The transformer ratio is calculated as 1.66 based on (5).

$$n = \frac{V_{bus\_min}}{V_{bat\_min}} \quad (5)$$

2) Optimizing the switching frequency range and DC-link capacitance. By calculating and evaluating the charger efficiency and power density, the switching frequency from 270 kHz to 315 kHz are chosen to minimize the DC-link capacitance that is 1320 μF.

2) Calculating the maximum LLC voltage gain with  $Q_{max}$  and  $R_{eq\_min}$ . In the optimized switching frequency range, the maximum LLC voltage gain is calculated as 1.1 based on  $R_{eq\_min} = 13.64 \Omega$ , the  $\lambda$  (ratio of  $L_m$  to  $L_r$ ) optimized as 4.54 and  $Q_{max} = 1.04$ .

3) Calculating the required maximum and minimum gain. The DC-link capacitance is 1320  $\mu\text{F}$ , the maximum  $\Delta V_{dc}$  is 33 V corresponding to 500 V DC-link voltage under 6.6 kW. The maximum gain and minimum gain can be calculated as

$$M_{\max} = \frac{V_{bus}}{V_{bus} - \frac{\Delta V_{\max}}{2}} \quad (6)$$

$$M_{\min} = \frac{V_{bus}}{V_{bus} + \frac{\Delta V_{\max}}{2}} \quad (7)$$

The required maximum gain and minimum gain are 1.034 and 0.968 so that the minimum LLC voltage gain is high enough to eliminate  $\Delta V_{dc}$ .  $Q_{\max}$  and  $\lambda$  are also proper to obtain high  $L_m$ .

4) Calculating the resonant network parameters. Based on  $\lambda$ ,  $Q_{\max}$  and  $R_{eq\_min}$ , the resonant parameters are calculated. From (8) and (9),  $L_m$  is 75  $\mu\text{H}$ ,  $L_r$  is 16.51  $\mu\text{H}$  and  $C_r$  is 17 nF.

$$\frac{1}{2\pi\sqrt{L_r C_r}} = f_r \quad (8)$$

$$\pi^2 \sqrt{\frac{L_r}{C_r}} / (8n^2 R_{eq\_min}) = Q_{\max} \quad (9)$$

## VI. EXPERIMENTAL VERIFICATION AND DISCUSSION

### A. Experimental Prototype

A prototype of bidirectional LLC charger using the SiC MOSFETs was built and illustrated in Fig. 13. Fig. 14 demonstrates the experimental platform. The rated charging and discharging power are 6.6 kW with 300-kHz LLC. The battery voltage ranges from 240 V to 420 V and the DC-link capacitors are the electrolytic capacitors as 1320  $\mu\text{F}$ . Other detailed parameters are given in TABLE III. The DSP of TMS32028377 from TI is adopted.

The power density is 56 W/in<sup>3</sup> and the water cooling can be used to cool the charger down. 1200 V 60 A SiC MOSFETs are used in  $Q_1 \sim Q_{13}$  and 650 V SiC MOSFETs are used in  $Q_{14} \sim Q_{16}$  based on TABLE I.

TABLE III  
KEY PARAMETERS OF PROTOTYPE

Quantity	Symbol	Parameters
Charging/Discharging power	$P_{charge}/P_{discharge}$	6.6 kW
PFC inductance	$L_{ac1}/L_{ac2}$	515 $\mu\text{H}$
PFC switching frequency	$f_{sw\_pfc}$	66.7 kHz
DC-link voltage	$V_{bus}$	400 V~700 V
DC-link capacitance	$C_{bus}$	1320 $\mu\text{F}$
Battery voltage	$V_{bat}$	240 V~420 V
LLC resonant frequency	$f_r$	300 kHz
LLC switching frequency range	$f_s$	270 kHz~315 kHz
Turns ratio	$n_1:n_2$	10:6
Magnetizing inductance	$L_m$	75 $\mu\text{H}$
Resonant inductance	$L_r$	16.51 $\mu\text{H}$
Resonant capacitance	$C_r$	17 nF
Output filter capacitance	$C_o$	60 $\mu\text{F}$

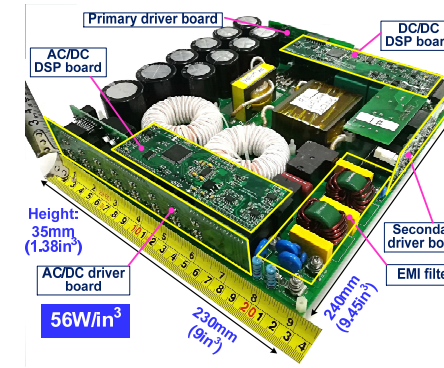


Fig. 13. Prototype of 6.6 kW bidirectional charger

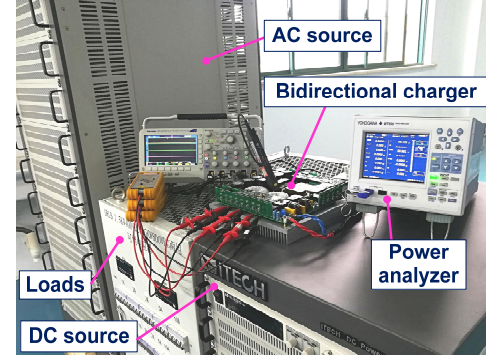


Fig. 14. Experimental platform for bidirectional charger

### B. Charging Mode Performance

Fig. 15 shows the grid voltage  $v_{ac}$ , the input current  $i_{Lac1}$  of single inductance in the PFC under 6.6 kW. The power factor is 0.994 and the THD of the input current is 3.43% with 360 V output and 6.6 kW. The FFT analysis meets IEEE-519 2014 shown in Fig. 16. When the LLC switching frequency is different from 300 kHz, the THD also does not change due to high switching frequency.

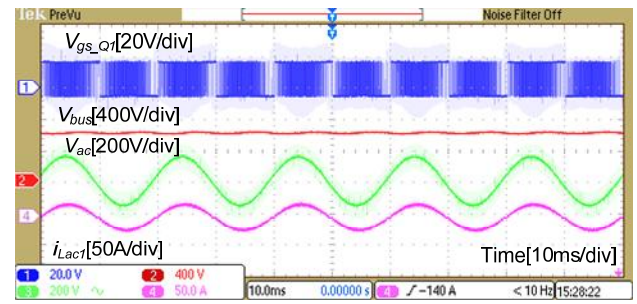


Fig. 15. AC-DC charge: grid current of single inductance with  $V_{bat}=360$  V,  $P_{charge}=6.6$  kW

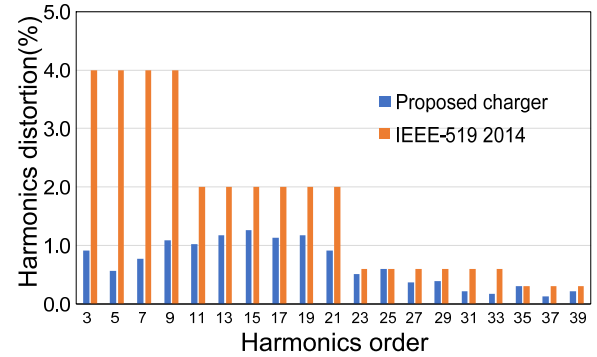


Fig. 16. Grid current FFT analysis with  $V_{bat}=360$  V,  $P_{charge}=6.6$  kW

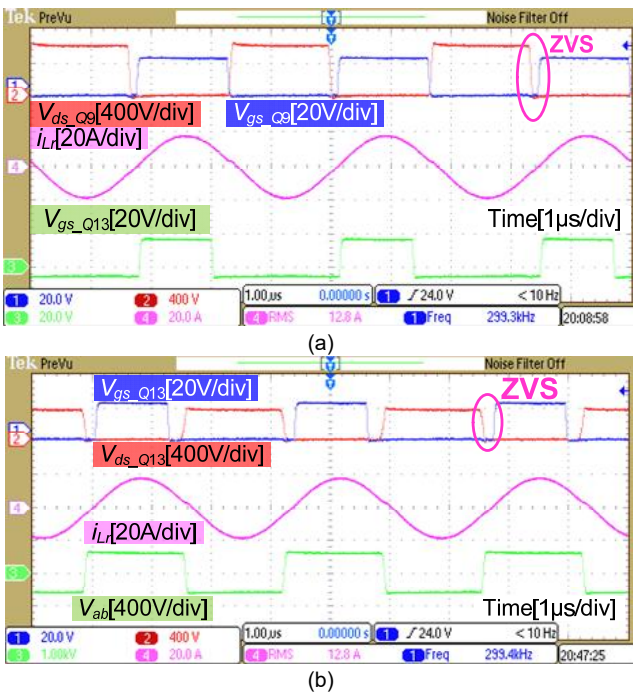


Fig. 17. DC-DC charge: ZVS turn-on with  $V_{bat}=360$  V,  $P_{charge}=6.6$  kW  
(a) ZVS in primary side (b) ZVS in secondary side

Fig. 17 shows the LLC waveforms with 360 V battery voltage at 300 kHz. It is observed that ZVS on both sides can be achieved to decrease the turn-on loss largely. The interval between the SR driving signals includes turn-on delay and turn-off delay, so that the secondary side ZVS is different from the primary side.

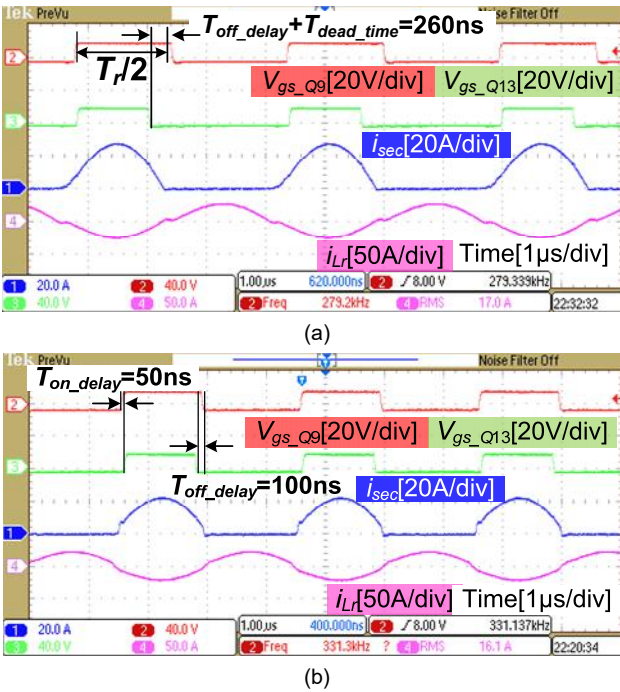


Fig. 18. SR implementation:  $V_{bat}=240$  V,  $P_{charge}=3.8$  kW (a)  $f_s=280$  kHz (b)  $f_s=330$  kHz

Fig. 18 shows the SR implementations at 240 V battery voltage and 3.8 kW based on the charging profile. The turn-on delay and turn-off delay are mainly based on the delay time of driver chip and buffer chip. When  $f_s$  is 280 kHz lower than  $f_r$ , the SR turns off ahead of the primary

driving signals. In order to prevent the resonant parameters to shift, the resonant frequency is 320 kHz and  $T_r/2$  is 1.56 μs. Based on (3), the SR conduction time is 1.25 μs shown as Fig. 18 (a). When  $f_s$  is 330 kHz higher than  $f_r$ , the turn-off time is ahead of the primary driving signals based on (4) and shown in Fig. 18 (b). Therefore, the proposed SR driving scheme can be conveniently implemented in the DSP.

Light load of 150 W (2% of 6.6 kW) is demonstrated in Fig. 19 with 280 kHz and critical ZCS. The SR on-time is lower than heavy loads. ZCS may be lost partially when the load continues to decrease based on the proposed SR scheme, however, the SR turn off current is very low and the loss is limited for the light load. It will not affect the control and hurt the efficiency for the proposed charger.

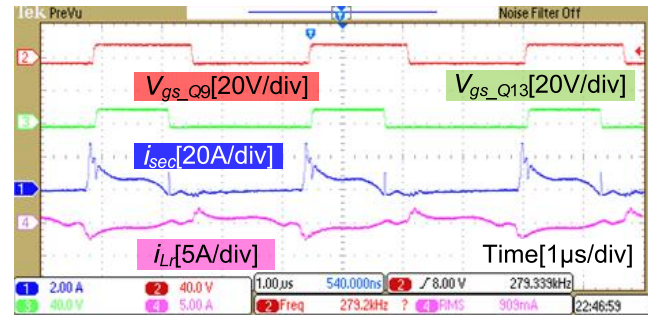


Fig. 19. SR waveform with  $P_{charge}=150$  W,  $f_s=280$  kHz,  $V_{bat}=240$  V

Fig. 20 demonstrates the voltage gain compensation control in charge.  $n$  denotes the transformer ratio and the value is 1.66. As the battery voltage is from 240 V to 300 V, the DC-link voltage is controlled from 400 V to 500 V gradually. It is observed that the DC-link voltage tracks the battery voltage so that the LLC operates around the resonant frequency to achieve high efficiency.

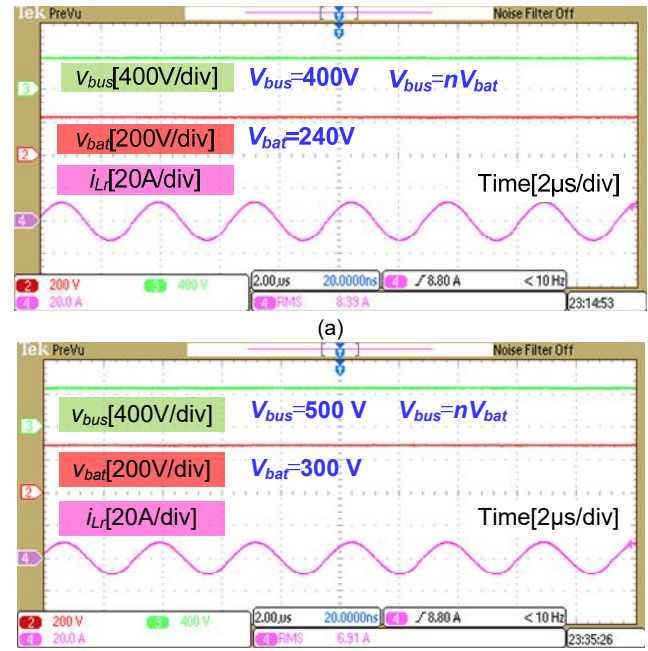


Fig. 20. Voltage gain compensation control under 2 kW (a)  $V_{bat}=240$  V and  $V_{bus}=400$  V (b)  $V_{bat}=300$  V and  $V_{bus}=500$  V

### C. Discharging Mode Performance

Fig. 21 demonstrates the reverse LLC waveforms in the discharge under 6.6 kW. The battery voltage is 350 V and both sides realize ZVS. Since the reverse LLC converter operates at 307 kHz, the resonant current is typically a sinusoidal waveform.

Fig. 22 shows the DC-AC waveforms and  $i_{ac}$  is the grid current. The DC-AC converter can achieve unity power factor and low grid current distortion.

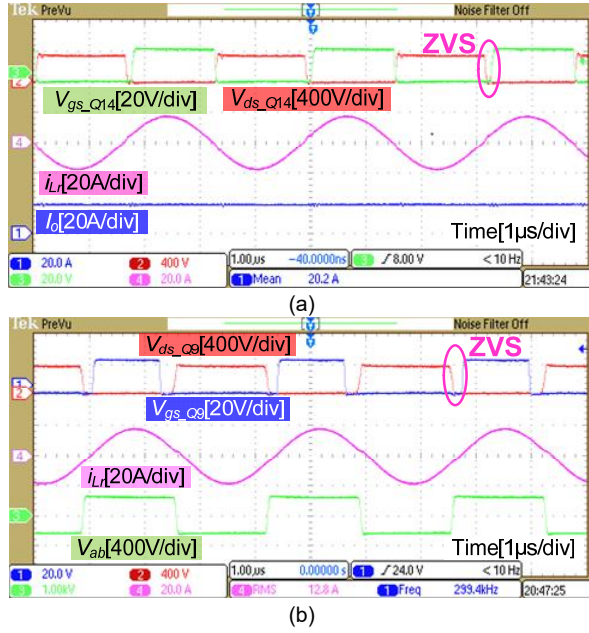


Fig. 21. DC-DC discharge with  $V_{bat}=350$  V,  $P_{discharging}=6.6$  kW (a) ZVS in secondary side (b) ZVS in primary side

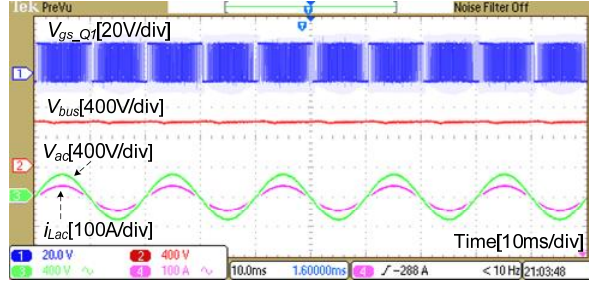


Fig. 22. DC-AC discharge:  $V_{bat}=350$  V,  $P_{discharge}=6.6$  kW

Fig. 23 shows the voltage gain compensation control in discharge. As  $V_{bat}$  is the minimum value of 240 V, the DC-link voltage is 391 V that is high enough for the input voltage of DC-AC converter to be grid-tied.

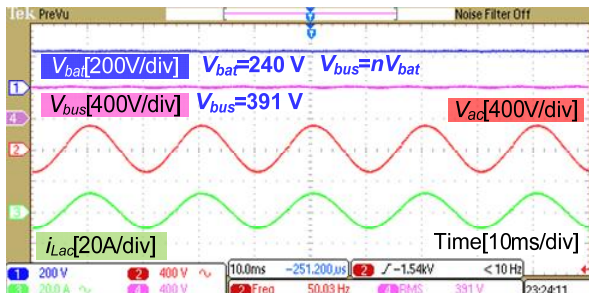


Fig. 23. Voltage gain compensation control in discharge under 2 kW

### D. Measured Efficiency

Fig. 24 gives the efficiencies in the charge. Based on the charging profile, the charging power is 5.1 kW at 270 V. The overall efficiency is above 96% in the entire battery voltage range.

The efficiency is higher for higher battery voltage when the loss increase of switching loss and transformer core loss is lower than the loss reduction of LLC conduction loss and transformer winding loss. While the efficiency is lower when the loss increase is higher than the loss reduction.

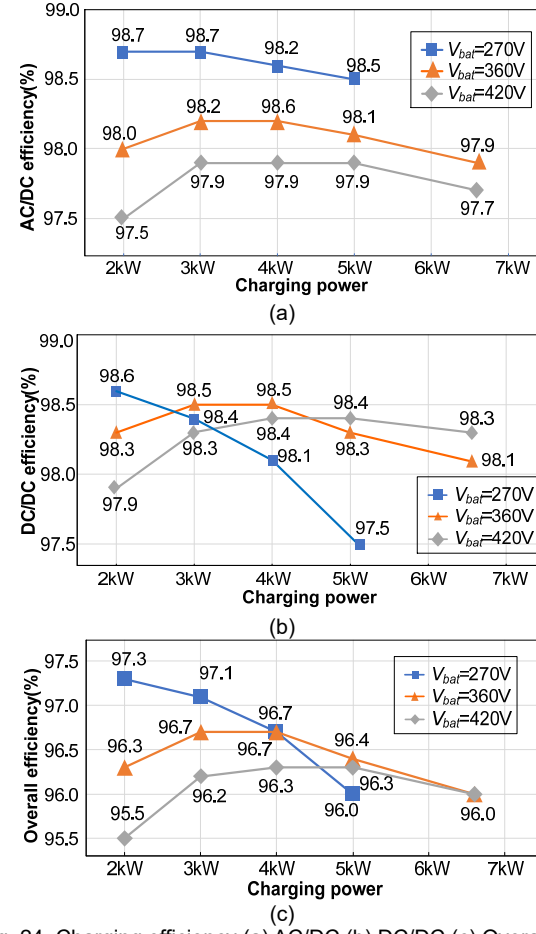


Fig. 24. Charging efficiency (a) AC/DC (b) DC/DC (c) Overall

TABLE IV gives the efficiency comparisons between the proposed charger and the state-of-the-art products. It should be noted that most of the products are unidirectional. The proposed bidirectional charger owns higher charging efficiency under 6.6 kW.

TABLE IV  
CHARGING EFFICIENCY COMPARISON BETWEEN PROPOSED CHARGER  
AND STATE-OF-THE-ART PRODUCTS

Part number	Vendor (Country)	Type	Efficiency (6.6 kW)
NLG664 [22]	Brusa (Switzerland)	Unidirectional	90%
BAIC7000T220A [23]	VMAX (China)	Unidirectional	93%
CAD332DF-400A [24]	Ovar (China)	Unidirectional	94%
CWBC Series 6.6 kW [25]	Current Ways (America)	Bidirectional	90%
Proposed charger	-	Bidirectional	96%

Based on [26], a 6.6 kW bidirectional charger was built from Wolfspeed. TABLE V shows the power density comparison between the proposed charger and Wolfspeed charger. The proposed charger efficiency is 0.6% higher than Wolfspeed. Moreover, the power density for the proposed charger is increased by 55.6% over the Wolfspeed design.

TABLE V  
COMPARISON BETWEEN PROPOSED CHARGER AND WOLFSPEED CHARGER

	L × W × H (mm)	Efficiency	Power density	Power density Increment
Wolfspeed charger	300×200×50	95.4%	36 W/in <sup>3</sup>	
Proposed charger	230×240×35	96%	56 W/in <sup>3</sup>	55.6%

In the discharge, the efficiencies are illustrated in Fig. 25. The peak overall efficiency under 6.6 kW is 96% and is 1% higher than the bidirectional state-of-the-art product from [25].

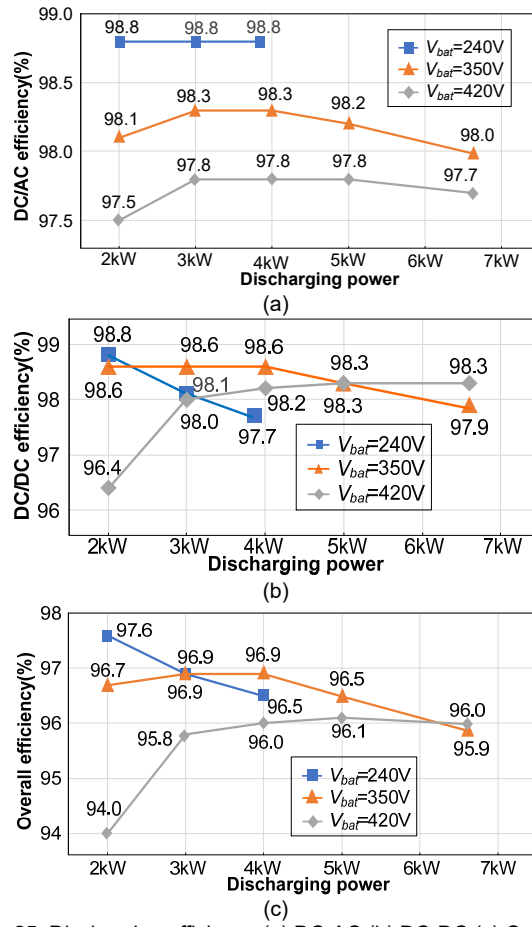


Fig. 25. Discharging efficiency (a) DC-AC (b) DC-DC (c) Overall efficiency

## VII. CONCLUSIONS

This paper proposed a SiC bidirectional LLC charger taking advantage of the LLC high efficiency and high power density. A voltage gain compensation control is proposed to enable the LLC bidirectional operation. The AC-DC stage adopts an interleaved bridgeless totem pole PFC to achieve unity power factor. Owing to the extra control freedom of DC-link voltage, the LLC voltage gain regulation can be shifted to the DC-AC stage. Furthermore, a digital adaptive SR

driving scheme based on the primary driver signals is also proposed. It improves the SR driving signals robust and is suitable for high voltage and high frequency application. An optimal LLC design is also presented to optimize the charger operation. Compared to the conventional LLC design, the proposed design only needs to design a low voltage gain to eliminate the double line frequency ripple and can obtain much higher magnetizing inductance to achieve high efficiency.

In the charge mode, the overall efficiency is above 96% over the entire battery voltage range, which is as much as 2% higher than the unidirectional state-of-the-art products and 0.6% higher than Wolfspeed charger even. Furthermore, the proposed bidirectional charger achieves the power density of 56 W/in<sup>3</sup> and increases 55.6% over the Wolfspeed solution. In the discharge mode, the peak overall efficiency under 6.6 kW is 96%, which is 1% higher than the bidirectional state-of-the-art products.

## REFERENCES

- [1] S. H. Ryu, D. H. Kim, M. J. Kim, J. S. Kim, and B. K. Lee, "Adjustable frequency-duty-cycle hybrid control strategy for full-bridge series resonant converters in electric vehicle chargers," *IEEE Trans. Ind. Electron.*, vol. 61, no. 10, pp. 5354–5362, Oct. 2014.
- [2] C.-Y. Oh, D.-H. Kim, D.-G. Woo, W.-Y. Sung, Y.-S. Kim, and B.-K. Lee, "A high-efficient non isolated single-stage on-board battery charger for electric vehicles," *IEEE Trans. Power Electron.*, vol. 28, no. 12, pp. 5746–5757, Dec. 2013.
- [3] M. Yilmaz, and P. T. Krein, "Review of battery charger topologies, charging power levels, and infrastructure for plug-in electric and hybrid vehicles," *IEEE Trans. Power Electron.*, vol. 28, no. 5, pp. 2151–2169, May 2013.
- [4] M. Kesler, M. C. Kisacikoglu, and L. M. Tolbert, "Vehicle-to-grid reactive power operation using plug-in electric vehicle bidirectional offboard charger," *IEEE Trans. Ind. Electron.*, vol. 61, no. 12, pp. 6778–6784, Dec. 2014.
- [5] M. Kwon and S. Choi, "An electrolytic capacitorless bidirectional EV charger for V2G and V2H applications," *IEEE Trans. Power Electron.*, vol. 32, no. 9, pp. 6792–6799, Sep. 2017.
- [6] R. Beiranvand, B. Rashidian, M. R. Zolghadri, and S. M. H. Alavi, "Using LLC resonant converter for designing wide-range voltage source," *IEEE Trans. Ind. Electron.*, vol. 58, no. 5, pp. 1746–1756, May 2011.
- [7] Z. Zhang, Y. Q. Wu, D. J. Gu and X. Ren, "Current ripple mechanism with quantization in digital LLC converters for battery charging applications," *IEEE Trans. Power Electron.*, Vol. 33, No. 2, pp. 1303–1312, Feb. 2018.
- [8] F. Musavi, M. Craciun, D. S. Gautam, and W. Eberle, "Control strategies for wide output voltage range LLC resonant DC-DC Converters in battery chargers," *IEEE Trans. Veh. Technol.*, vol. 63, no. 3, pp. 1117–1125, Mar. 2014.
- [9] F. Krämer and J. W. Kolar, "Accurate power loss model derivation of a high-current dual active bridge converter for an automotive application," *IEEE Trans. Ind. Electron.*, vol. 57, no. 3, pp. 881–891, Mar. 2010.
- [10] J. Park and S. Choi, "Design and control of a bidirectional resonant dc-dc converter for automotive engine/battery hybrid power generators," *IEEE Trans. Power Electron.*, vol. 29, no. 7, pp. 3748–3757, Jun. 2014.
- [11] W. Chen, P. Rong, and Z. Lu, "Snubberless bidirectional DC-DC converter with new CLLC resonant tank featuring minimized switching loss," *IEEE Trans. Power Electron.*, vol. 57, no. 9, pp. 3075–3086, Sep. 2010.
- [12] Z. U. Zahid, Z. M. Dalala, R. Chen, B. Chen, and J.-S. Lai, "Design of bidirectional DC-DC resonant converter for vehicle-to-grid (V2G) applications," *IEEE Trans. Transportation Electrification*, vol. 1, no. 3, pp. 232–244, Oct. 2015.
- [13] M.-H. Ryu, H.-S. Kim, J.-W. Baek, H.-G. Kim, and J.-H. Jung, "Effective test bed of 380-V DC distribution system using isolated power converters," *IEEE Trans. Ind. Electron.*, vol. 62, no. 7, pp. 4525–4536, Jul. 2015.
- [14] B. Li, F. C. Lee, Q. Li, and Z. Liu, "Bi-directional on-board charger architecture and control for achieving ultra-high efficiency with wide battery voltage range," in *Proc. IEEE Appl. Power Electron. Conf. Expo.*, Mar. 2017, pp. 3688–3694.

- [15] C. Shi, H. Wang, and A. Khaligh, "A SiC based PEV onboard charger with ultra-wide DC link voltage range," *IEEE Trans. Ind. Appl.*, vol. 52, no. 4, pp. 3461–3471, Apr. 2016.
- [16] B. Whitaker, A. Barkley, Z. Cole, B. Passmore, D. Martin, T. McNutt, A. B. Lostetter, J. S. Lee and K. Shiozaki, "A high-density, high-efficiency, isolated on-board vehicle battery charger utilizing silicon carbide power devices," *IEEE Trans. Power Electron.*, vol. 29, no. 5, pp. 2606–2617, May 2014.
- [17] H. R. Li, L. Bai, Z. Zhang, S. D. Wang, J. C. Tang, X. Y. Ren, and J. F. Li, "A 6.6kW SiC bidirectional on-board charger" in *Proc. IEEE Appl. Power Electron. Conf. Expo.*, Mar. 2018, pp. 1171–1178.
- [18] L. Xue, Z. Shen, D. Boroyevich, P. Mattavelli, and D. Diaz, "Dual active bridge-based battery charger for plug-in hybrid electric vehicle with charging current containing low frequency ripple," *IEEE Trans. Power Electron.*, vol. 30, pp. 7299–7307, Dec. 2015.
- [19] X. Wu, G. Hua, J. Zhang, and Z. Qian, "A new current-driven synchronous rectifier for series-parallel resonant (LLC) DC-DC converter," *IEEE Trans. on Ind. Electron.*, vol. 58, no. 1, pp. 289–297, Jan. 2011.
- [20] On semiconductor. Secondary Side Synchronous Rectification Driver for High Efficiency SMPS Topologies. [Online]Available: <http://www.onsemi.cn/pub/Collateral/NCP4305-D.PDF>
- [21] H. Wang, S. Dusmez, and A. Khaligh, "Maximum efficiency point tracking technique for LLC-based PEV chargers through variable dc link control," *IEEE Trans. Ind. Electron.*, vol. 61, no. 11, pp. 6041–6049, Nov. 2014.
- [22] Brusa. BRUSA\_DB\_EN\_NLG664. [Online]Available: [https://www.brusa.biz/fileadmin/template/Support-Center/Datenbl%C3%A4tter/BRUSA\\_DB\\_EN\\_NLG664.pdf](https://www.brusa.biz/fileadmin/template/Support-Center/Datenbl%C3%A4tter/BRUSA_DB_EN_NLG664.pdf)
- [23] SHENZHEN VMAX POWER Co., Ltd. BAIC7000T220A (Low Voltage). [Online]Available: <http://www.Vmaxpower.com.cn/Upfiles/filedown/2015101055871.pdf>
- [24] Ovar Technology Co., Ltd. On-board 6.6kW Liquid-Cooled Charger (200–420VDC). [Online]Available: <http://www.ovartech.com/wp-content/uploads/2017/12/6.6kW-charger-CAD662DF-400A.pdf>
- [25] CURRENTWAYS TECHNOLOGIES. CWBC Series 6.6kW Bi-directional EV On Board Charger. [Online]Available: <http://www.currentways.com/wp-content/uploads/2013/10/CWBC-Serie-s-6.6kW-Bi-directional-charger-Liquid-Cooled-050918.pdf>
- [26] Wolfspeed Corp. 6.6 kW BI-DIRECTIONAL EV ON-BOARD charger. [Online]Available: [http://go.wolfspeed.com/l/101562/2018-07-13/5582c6/101562/71213/CRD\\_06600FF10N\\_Presentation.pdf](http://go.wolfspeed.com/l/101562/2018-07-13/5582c6/101562/71213/CRD_06600FF10N_Presentation.pdf)



**Haoran Li** (S'17) received the B.S. degree in Electrical Engineering from Anhui University, Hefei, P. R. China, in 2013. He received the M.S. degree in Electrical Engineering from Shanghai University of Electric Power, Shanghai, P. R. China, in 2016. He is currently working toward the Ph.D. degree at the Aero-Power Sci-Tech Center, Nanjing University of Aeronautics and Astronautics (NUAA). His research interests include high frequency SiC applications and digital control techniques for the Electric Vehicle (EV) charger.

**Zhiliang Zhang** (S'03–M'09–SM'14) received the B.Sc. and M.Sc. degrees from Nanjing University of Aeronautics and Astronautics (NUAA), P. R. China, in 2002 and 2005, and Ph.D. degree from Department of Electrical and Computer Engineering, Queen's University, Kingston, ON, Canada, in 2009. From June to September 2007, he was a Design Engineering Intern from with Burlington Design Center, Linear Technology Corporation. He is currently a Professor with the Aero-Power Sci-Tech Center, NUAA. He was a Secretary of PELS TC on Power and Control Core Technologies from 2013 to 2016. He authored or coauthored 40 papers in IEEE TRANSACTIONS ON POWER ELECTRONICS, and more than 70 papers in IEEE conferences. He holds 12 China patents and one U.S. patent. He coauthored the book High Frequency MOSFET Gate Drivers: Technologies and Applications (IET, 2017). His research interests include high-frequency power conversion with wide bandgap devices.



Dr. Zhang was a Winner of "United Technologies Corporation Rong Hong Endowment" in 1999. He was the recipient of National Excellent Youth Fund from National Natural Science Foundation of China in 2017. He serves as an Associate Editor of IEEE Journal of Emerging and Selected Topics of Power Electronics (IEEE JESTPE) from July, 2018. He was a Guest Associate Editor for special issue of JESTPE: Resonant and Soft-Switching Techniques with Wide Bandgap Devices in 2018; Power Integration with WBG Devices and Components, 2019 respectively.



**Shengdong Wang** received the B.S. and M.S. degrees in Electrical Engineering from Jiangsu University, Zhenjiang, P. R. China, in 2011, and 2014, respectively. He is currently working toward the Ph.D. degree at the Aero-Power Sci-Tech Center, Nanjing University of Aeronautics and Astronautics. His research interests include bidirectional ac–dc conversion, high frequency applications of wide bandgap devices and digital control techniques for the Electric Vehicle (EV) charger.



**Jiacheng Tang** received the B.S. degree in Electrical Engineering from Nanjing University of Aeronautics and Astronautics, Nanjing, P. R. China, in 2017. He is currently working toward the M.S. degree at the Aero-Power Sci-Tech Center, Nanjing University of Aeronautics and Astronautics. His research interests include high frequency SiC applications and magnetic components for power electronic circuits.



**Xiaoyong Ren** (S'04–M'11) received the B.S., M.S. and Ph.D. degrees in Electrical Engineering from NUAA, Nanjing, P. R. China, in 2002, 2005 and 2008, respectively. From 2009 to 2011, he was a Postdoctoral Researcher at the Center for Power Electronics Systems, Virginia Polytechnic Institute and State University, Blacksburg, VA, USA. He is currently with the Department of Electrical Engineering, NUAA. His current research interests include dc–dc conversion, converter control techniques, GaN device application and renewable power systems.



**Qianhong Chen** (M'06) received the B.S. and Ph.D. degrees in electrical engineering from NUAA, Nanjing, P. R. China, in 1995, 1998 and 2001, respectively. She is currently a Professor with the Aero-Power Sci-Tech Center. Her research interests include application of integrated-magnetics, wireless power transfer. Dr. Chen is the director of the NUAA-ZTE Joint Laboratory of the communication wireless power transmission technology and one of the main sponsors of the high-power wireless transmission industry alliance in China.